Relativistic effects in photoionization time delay near the Cooper minimum of noble gas atoms

Soumyajit Saha[1], Ankur Mandal[1], Jobin Jose[2], Hari R. Varma[3], P. C. Deshmukh[1,7], A. S. Kheifets[4], V. K. Dolmatov[5] and S. T. Manson[6]
[1] *Department of Physics, Indian Institute of Technology Madras, Chennai-600036, India*
[2] *Department of Chemistry, Texas A & M University, College Station, Texas, USA*
[3] *School of Basic Sciences, Indian Institute of Technology, Mandi, 175001, India*
[4] *Research School of Physics and Engineering, The Australian National University, Canberra ACT 0200, Australia*
[5] *Department of Physics and Earth Science, University of Northern Alabama, Florence, AL 35632, USA*
[6] *Department of Physics and Astronomy, Georgia State University, Atlanta, 30303, U.S.A. and*
[7] *Department of Physics and Astronomy, The University of Western Ontario, London, Canada, N6A 3K7*
(Dated: September 16, 2014)

Time delay of photoemission from valence ns, $np_{3/2}$ and $np_{1/2}$ sub-shells of noble gas atoms is theoretically scrutinized within the framework of the dipole relativistic random phase approximation. The focus is on the variation of time delay in the vicinity of the Cooper minima in photoionization of the outer sub-shells of neon, argon, krypton and xenon, where the corresponding dipole matrix element changes its sign while passing through a node. It is revealed that the presence of the Cooper minimum in one photoionization channel has a strong effect on time delay in other channels. This is shown to be due to inter-channel coupling.

PACS numbers: 32.80.Rm 32.80.Fb 42.50.Hz

I. INTRODUCTION

Time delay in atomic photoionization refers to a slight temporal delay in the release of the photoelectron wave-packet upon absorption of a short electromagnetic pulse. This delay is very small, of the order of attoseconds (as). This opens a unique road towards calibration of various measuring devices that can capture electron motion in atoms, molecules and solids on the attosecond time scale that would be difficult to do otherwise. These devices are known as attosecond streak camera [1, 2], the angular streaking attoclock [3] and the RABITT (Reconstruction of Attosecond Bursts by Ionization of Two-photon Transitions) [4]. In these devices, the phase stabilized electric field of a short laser pulse is used to convert the release time of the outgoing electron wavepacket into other measurable quantities such as the kinetic energy (attosecond streak camera), the momentum vector (angular streaking attoclock) or the beating signal of the electron detector (RABITT).

To date, the relative time delay of photoemission from neighboring valence atomic sub-shells has been measured with a high accuracy in neon [5] and argon [4, 6]. The relative time delay between the outer shells of the atomic pairs (He vs. Ne and Ne vs. Ar) can now be determined owing to active stabilization of the RABITT spectrometer [7]. Similar measurement can be performed in heavier noble gas atoms relative to the time delay in the $1s$ sub-shell of He [8]. The high harmonics generation (HHG) technique has also been used to determine the time delay in Ar [9].

The concept of time-delay was introduced in the early works Eisenbud [10] and Wigner [11] in the context of the phase shift analysis of slow electron s-wave scattering. The focus of the Eisenbud-Wigner theory was the group velocity of a wave-packet [12]. Typically, a free-electron wave-packet, which is made up from the superposition of plane waves with different energies $E = k^2/2$, emerging at a point x_0, spreads with time, even in vacuum (note the use of atomic units in which $e = m = \hbar = 1$ throughout the paper). Its peak propagates at the group velocity $v_g = d\omega/dk\big|_{k=k_0}$. Here, k_0 is the mean momentum of the free electron that contributes to the wave-packet. When the free-electron wave-packet elastically scatters off a potential, a peak of the transmitted wave-packet propagates at the *same* group velocity $v_g = d\omega/dk\big|_{k=k_0}$ as before scattering. The corresponding transmission amplitude T is generally complex, $T = |T|\, e^{i\varphi_T}$, with φ_T being the amplitude's phase. Due to the phase factor in T, the transmitted wave-packet appears to have originated at a *different* point, namely, at $x_0 - d\varphi_T/dk\big|_{k_0}$, rather than at x_0. The term $d\varphi_T/dk\big|_{k_0}$ in the above expression determines the *spatial* phase shift $x_{\rm shift} = d\varphi_T/dk\big|_{k_0}$. It provides a measure for the time delay $t_{\rm delay}$ due to electron scattering:

$$t_{\rm delay} = \frac{x_{\rm shift}}{v_g} = \frac{d\varphi_T/dk\big|_{k_0}}{d\omega/dk\big|_{k=k_0}} = \frac{d\varphi_T}{dE}\Big|_{E_0}, \qquad (1)$$

where E_0 is the mean energy of the wave-packet. As shown earlier [13], time delay in a collision process, defined in terms of an energy-derivative of the phase shift, is the same as collision life-time. Therefore, the former serves as a temporal measure of the complex system which emerges due to photoabsorption and the subsequent decay by emitting a photoelectron from the atomic complex. In recent years, accurate numerical calculation of atomic time delay has become an *ad hoc* topic of intense theoretical studies [14–18].

II. METHODOLOGY

In the present paper, atomic photoionization is calculated using *incoming boundary conditions* for the final continuum state wave functions. These ion-plus-photoelctron final states are related to the wave function for elastic electron-ion scattering through time-reversal symmetry [19]. In the relativistic random phase approximation (RRPA), an electron transition due to photoionization is described by a dipole matrix element which is generally complex [20, 21]. In particular, for a transition from an initial bound state $|n,\kappa\rangle$ to a continuum state $|E,\overline{\kappa}\rangle$, the dipole matrix element is given by

$$\langle E,\overline{\kappa}|\,\hat{d}\,|n\kappa\rangle = i^{1-\overline{\ell}}e^{i\delta_{\overline{\kappa}}}\langle E,\overline{\kappa}\|Q_1^{(1)}\|n\kappa\rangle\ . \qquad (2)$$

Here, $\langle E,\overline{\kappa}\|Q_1^{(1)}\|n\kappa\rangle$ is the reduced matrix element and $\delta_{\overline{\kappa}}$ is the phase shift of the final-state continuum wave function with incoming boundary conditions. Since the photoionization matrix element is generally complex, the energy-dependent phase shifts $\delta_{\overline{\ell}}(E)$ of a partial ℓ-electronic wave is defined by

$$\delta_{\overline{\ell}}(E) = \tan^{-1}\left\{\frac{\mathrm{Im}\langle E,\overline{\kappa}|\,\hat{d}\,|n\kappa\rangle}{\mathrm{Re}\langle E,\overline{\kappa}|\,\hat{d}\,|n\kappa\rangle}\right\} \qquad (3)$$

The quantity $d\delta_{\overline{\ell}}(E)/dE$ then provides a measure of time-delay occurring in various dipole photoionization channels.

Ab-initio RRPA [20, 21] accounts, reliably, both for relativistic effects, such as the initial and final state spin-orbit splitting, and major many-body correlations. The latter are particularly important to the calculations of this paper since phase shifts $\delta_{\overline{\ell}}(E)$ are known to be quite sensitive to correlation in the form of inter-channel coupling. Therefore a reliable accounting for this aspect of correlation is vital for an adequate study of the time delay phenomenon.

In the present RRPA calculations of photoionization matrix elements and photoelectron phase shifts, experimental ionization thresholds were substituted into the RRPA equations. Corresponding ionization thresholds for Ne, Ar, Kr, and Xe are presented in Table 1. Furthermore, the following number of relativistic dipole photoionization channels were accounted for in corresponding RRPA calculations of photoionization of these atoms: (a) for Ne - 7 channels which originate due to photoionization of the $2p$ and $2s$ sub-shells; (b) for Ar - 14 channels (from $3p$, $3s$, $2p$ and $2s$ sub-shells), whereas (c) both for Kr and Xe 13 channels (from the $4p$, $4s$, $3d$ sub-shells of Kr and $5p$, $5s$, $4d$ sub-shells of Xe) were coupled in the *truncated* RRPA. Note that the omitted channels, being far away energetically, should be unimportant in the energy ranges considered; this is substantiated by the excellent agreement between the length and velocity forms of the dipole matrix elements.

TABLE I: Dirac-Hartree-Fock (DHF) and experimental [22] sub-shell thresholds

Atom	Sub-shell	DHF a.u.	Expt. a.u.
Ne	$2p_{\frac{3}{2}}$	0.848	0.794
	$2p_{\frac{1}{2}}$	0.853	0.797
	$2s$	1.936	1.948
Ar	$3p_{\frac{3}{2}}$	0.588	0.579
	$3p_{\frac{1}{2}}$	0.595	0.586
	$3s$	1.287	1.077
	$2p_{\frac{3}{2}}$	9.547	
	$2p_{\frac{1}{2}}$	9.631	
	$2s$	12.411	
Kr	$4p_{\frac{3}{2}}$	0.514	0.514
	$4p_{\frac{1}{2}}$	0.542	0.540
	$4s$	1.188	1.010
	$3d_{\frac{5}{2}}$	3.727	
	$3d_{\frac{3}{2}}$	3.777	
Xe	$5p_{\frac{3}{2}}$	0.439	0.444
	$5p_{\frac{1}{2}}$	0.493	0.492
	$5s$	1.0101	0.859
	$4d_{\frac{5}{2}}$	2.634	
	$4d_{\frac{3}{2}}$	2.711	

III. RESULTS AND DISCUSSION

A. Photoionization cross-sections, phase shifts and time delays

In this section, RRPA calculated results for the photoionization cross sections, phase shifts and time delays in valence shells of Ne, Ar, Kr and Xe are presented. Moreover, in order to understand the importance of relativistic effects, these results are compared with corresponding calculated results of work [17] which were obtained, as in [23], within the framework of a non-relativistic random phase approximation (RPAE [24]). In this way, the role of relativistic effects will be elucidated in a consistent manner in view of the complete equivalency between RPAE and RRPA in accounting both for direct and exchange interactions; the only difference in the two methodologies is the inclusion of relativistic effects in the RRPA. In RPAE, the expression for the photoionization amplitude is given by

$$f_{n_il_i}(E) \ \propto \sum_{\substack{l=l_i\pm1\\ m=m_i}} e^{i\delta_l} i^{-l} Y_{lm}(\hat{k})\,(-1)^m \begin{pmatrix} l & 1 & l_i \\ -m & 0 & m_i \end{pmatrix} \times \langle El\|D\|n_il_i\rangle. \qquad (4)$$

Here, the reduced dipole matrix element, which is stripped of all the angular momentum projections, is defined as

$$\langle El\| \, r \, \|n_i l_i\rangle = \hat{l}\hat{l}_i \begin{pmatrix} l & 1 & l_i \\ 0 & 0 & 0 \end{pmatrix} \int r^2 dr \, R_{El}(r) \, r \, R_{n_i l_i}(r) \ , \tag{5}$$

where $\hat{l} \equiv \sqrt{2l+1}$. In the present work, the amplitude $f(E)$ is evaluated in the forward direction $k\|\hat{z}$, which is usually the case in the attosecond time delay measurements. In the relativistic case, we use the same expression (4) in which the orbital momenta of the initial bound state and the final continuum state are substituted by their relativistic counterparts $\ell \to j = \ell + 1/2$.

The photoelectron group delay, which is the energy derivative of the phase of the complex photoionization amplitude, gives an alternative access to the phase information. It is evaluated as

$$\tau = \frac{d}{dE} \arg f(E) \equiv \mathrm{Im}\Big[f'(E)/f(E)\Big] \ . \tag{6}$$

Note that when a single channel dominates, the time delay (6) reduces to the energy derivative of the phase of that channel. However, in the general case, when more than one amplitude contributes materially to the cross section from a given initial state, the phase in question is the phase of the photoionization amplitude (4). The derivative of that phase is the essence of the time delay. In other words, the phase is essentially a weighted average of the phases of the respective channels. The time delay, thus, is a weighted average of the individual channel time delays. Furthermore, in such case, Eq. (4) shows that the time delay is angular dependent.

1. *Neon*

On the top panel of Fig. 1 we present the partial photoionization cross-sections of valence shell photoionization of Ne. The RRPA cross-sections are shown by the solid (red) lines and the RPAE cross-sections are exhibited by the dashed (blue) line. The recommended experimental data by Bizau and Wuilleumier [25] are displayed by filled circles with error bars. On the middle panel, we use the same line style to show the phases of the photoionization amplitudes $f_{2s}(E)$ and $f_{2p}(E)$ evaluated in the $\hat{z}$ direction. The bottom panel of Fig. 1 displays the photoelectron group delay calculated as the energy derivative of the phase of the corresponding photoionization amplitude evaluated in the z-axis direction. Photoemission from the $2s$ sub-shell seems to be ahead of that of the $2p$ sub-shell at around 100 eV photon energy mark where the measurement of Schultze *et al* [5] was taken (shown as a vertical bar in the figure).

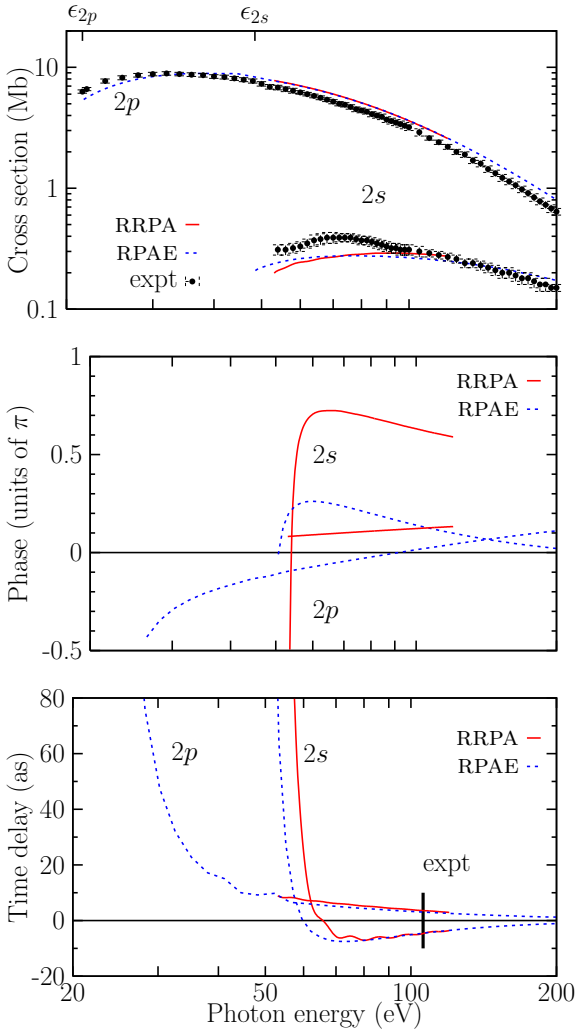

FIG. 1: (Color online) Top: the partial photoionization cross-sections of the $2s$ and $2p$ sub-shells of Ne. The RRPA and RPAE calculations are shown by the solid (red) and dashed (blue) lines, respectively. The recommended experimental data by Bizau and Wuilleumier [25] are displayed by filled circles with error bars. Middle: phases in the photoionization amplitudes $\arg f_{2s}(E)$ and $\arg f_{2p}(E)$ evaluated in the $\hat{z}$ direction. The same line styles are used for the RPAE and RRPA calculations. Bottom: the phase derivatives are converted into the units of the group delay. The length of the vertical bar at the photon energy of 106 eV visualizes the relative time delay between the $2p$ and $2s$ sub-shells of 21 ± 5 as as measured by Schultze *et al* [5]

2. *Argon*

An analogous set of data for Ar $3s$ and $3p$ sub-shells is shown in Fig. 2. On the top panel we make a comparison of the RRPA (solid red line) and RPAE (dashed blue line) partial photoionization cross-sections with the experimental data by Möbus *et al* [26] for $3s$ sub-shell and by Samson and Stolte [27] for the sum of $3s$ and $3p$ sub-shells. These partial photoionization cross-sections

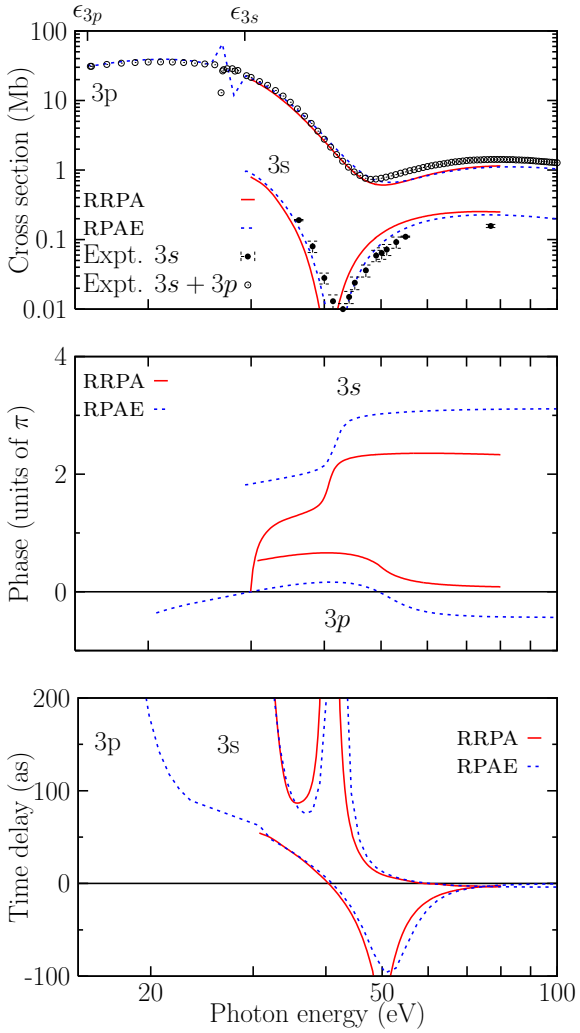

FIG. 2: (Color online) Top: the partial photoionization cross-sections of the $3s$ and $3p$ sub-shells of Ar. The RPAE and RRPA calculations are shown by the dashed (blue) and solid (red) lines, respectively. The experimental data for $3s$ [26] and for $3s + 3p$ [27] are displayed by filled circles with error bars and open circles, respectively. Middle: phases in the photoionization amplitudes $\arg f_{3s}(E)$ and $\arg f_{3p}(E)$ evaluated in the $\hat{z}$ direction. The same line styles are used for the RPAE and RRPA calculations. Bottom: the phase derivatives are converted into the units of the group delay.

are qualitatively different from those of Ne shown in Fig. 1. Firstly, the $3p$ cross-section in Ar displays the Cooper minimum whereas the nodeless $2p$ orbital does not [28]. Second, the inner-shell correlation changes completely the $3s$ cross section in magnitude and shape and introduces a deep Cooper-like minimum at a slightly smaller photon energy. Both the RRPA and RPAE calculations reproduce these features in fair agreement with the experiment. We note that the total cross-section measurement of Samson and Stolte [27] includes ionization leading to the ionic ground state as well as ionization with excitation. The former process, not included in the present calculations, seems to be insignificant as can be seen by a good agreement between the both theories and the experiment. This also means that the total cross section is dominated by the $3p$ shell in this energy region.

The RRPA and RPAE phases in Ar, shown in the middle panel of Fig. 2 are very different from Ne. When the cross-section goes through the Cooper minimum, the corresponding phase makes a jump of about π in the $3s \to \varepsilon p$ amplitude, and $-\pi$ in the $3p \to \varepsilon d$ amplitude. This jump is easy to understand. If the amplitude was real and had a node, it would simply change its sign which would amount to adding a phase factor of π in the complex number representation.

This jump of π has a dramatic effect on the time delay which is shown on the bottom panel of Fig. 2. It drives the time delay in the $3s$ sub-shell to very larger numbers of the order of several hundreds of attoseconds. The situation is less dramatic for the $3p$ sub-shell. Here the normally weak transition $3p \to \varepsilon s$ takes over near the Cooper minimum of the strong $3p \to \varepsilon d$ transition and the resulting time delay does not go below -100 as in the RPAE calculation. This minimum is somewhat deeper in the RRPA calculation.

Note that the Cooper minimum in the $3s$ photoionization channel in the 50 eV region arises solely due to inter-channel coupling with the $3p$ photoionization channels [29]. Thus, the change of phase by $\sim \pi$ in the $3s$ channel, and the resultant huge time delay, is part and parcel of the "transfer" of the Cooper minimum from the $3p$ to the $3s$ channels via correlation in the form of inter-channel coupling.

3. *Krypton*

On the top panel of Fig. 3, we display the partial photoionization cross-sections of the $4s$, $4p$ and $3d$ subshells of Kr calculated in the RRPA and RPAE models (shown by the solid (red) and dotted (blue) lines, respectively. Note that the energy regions around 27.48 eV ($4s_{1/2}$ threshold) and from 101.41eV ($3d_{5/2}$ threshold) to 102.80 eV ($3d_{3/2}$ threshold) are skipped because they fall into the region of autoionization resonances. Comparison is made with the experimental data by Ehresmann et al. [30] for $4s$ (displayed by filled circles with error bars), by Samson and Stolte [27] for the total $4s + 4p + 3d$ cross-section (shown by open circles), and by Aksela et al. [31] for $3d$ (displayed with asterisks). Good agreement between the two calculations can be seen for the $4p$ and $3d$ sub-shells which dominate the total cross-section in their respective energy ranges. The Cooper minimum of the $4s$ sub-shell is slightly displaced between the two calculations.

On the middle panel of Fig. 3 we display the phases of the photoionization amplitudes calculated in the same two models. Here agreement is not so close as for the cross-section. This demonstrates a greater sensitivity of the phase of the matrix elements to the details of the cal-

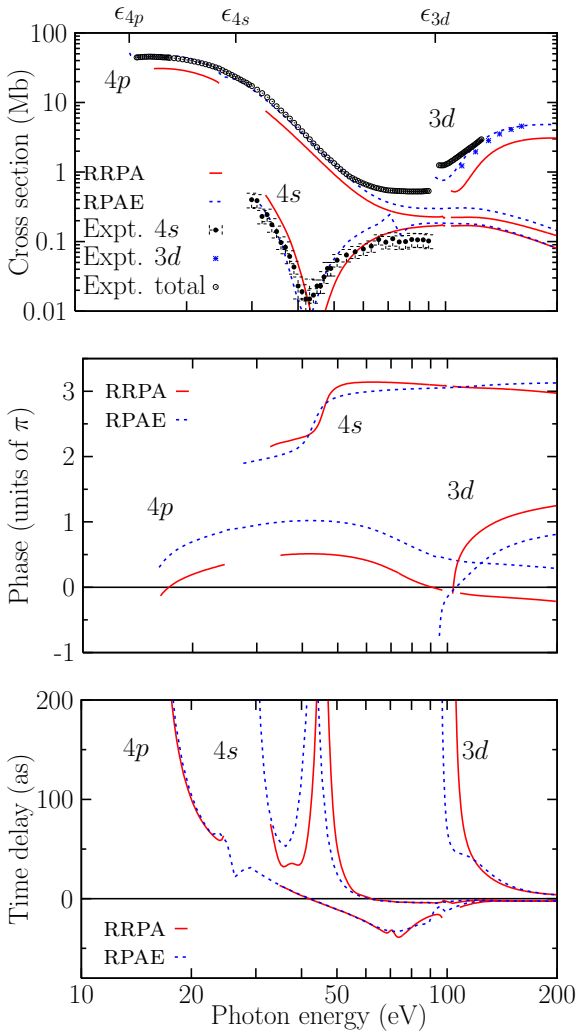

FIG. 3: (Color online) Top: the partial photoionization cross-sections of Kr. The RRPA and RPAE calculations are shown by the solid (red) and dashed (blue) lines, respectively. The experimental data by Ehresmann et al. [30] for $4s$ are displayed by filled circles with error bars and the total cross-section data by Samson and Stolte [27] are shown with open circles. The data from Aksela et al. [31] for $3d$ are displayed with asterisks. Middle: phases in the photoionization amplitudes evaluated in the $\hat{z}$ direction. The same line styles are used for the RPAE and RRPA calculations. Bottom: the phase derivatives are converted into the units of the time delay.

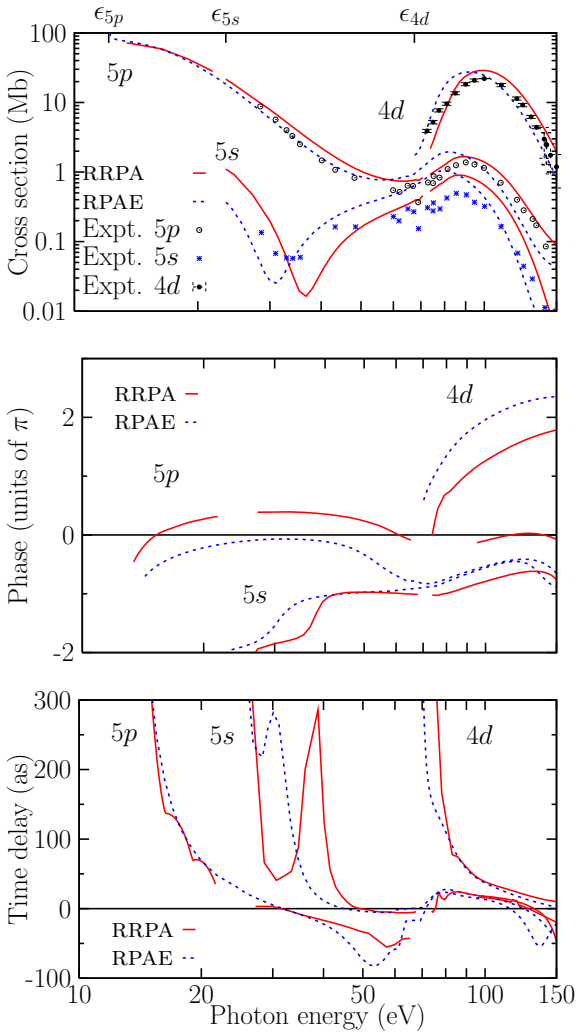

FIG. 4: (Color online) Top: the partial photoionization cross-sections of Xe. The RRPA and RPAE calculations are shown by the solid (red) and dashed (blue) lines, respectively. The experimental data for the $5p$ shell by Becker *et al* [32] and Fahlman et al. [33] are shown with open circles. The experimental data of the same authors for the $5s$ shell are shown with asterisks. The experimental data by Becker *et al* [32] and Lindle et al. [34] for the $4d$ shell are shown by filled circles with error bars. Middle: the partial photoionization phase shifts for the $5s$, $5p$ and $4d$ channels. Bottom: the phase derivatives are converted into the units of the time delay.

culation in comparison with their squared moduli (cross-sections).

On the bottom panel of Fig. 3 the phase shifts are converted into photoemission time delays according to Eq. (6). The time delays are qualitatively similar in the two models. However, some important differences can be clearly seen. More specifically, the sharp peak in the $4s$ time delay near the Cooper minimum of the partial photoionization cross-section is shifted between the two calculations.

4. *Xenon*

On the top panel of Fig. 4 we display the partial photoionization cross-sections of the $5s$, $5p$ and $4d$ subshells of Xe calculated in the RRPA (red solid lines) and RPAE (blue dashed lines) models. Note that the energy regions around 23.37 eV ($5s_{1/2}$ threshold) and from 71.66eV ($4d_{5/2}$ threshold) to 73.77 eV ($4d_{3/2}$ threshold) are skipped because because they fall into the region of autoionization resonances. Comparison is made with the experimental data from Becker *et al* [32] and Fahlman

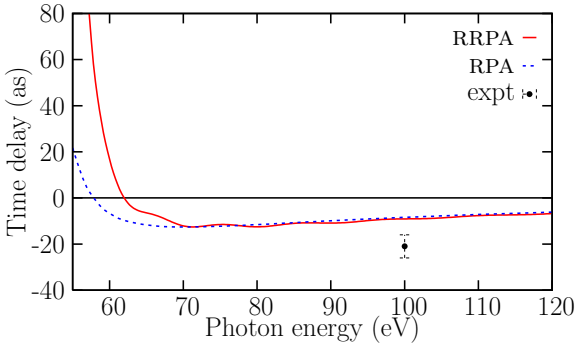

FIG. 5: The time delay difference between the $2s$ and $2p$ sub-shells of neon in the RRPA and RPAE calculations. The experimental data point (filled square with error bar) is from [5].

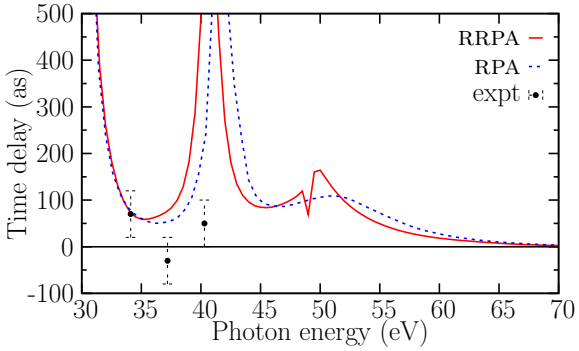

FIG. 6: The time delay difference between the $3s$ and $3p$ sub-shells of argon. The non-relativistic RPAE calculation (blue solid line) is from [17]. The experimental data (filled circles with error bars) are from [6].

et al. [33] for the $5s$ and $5p$ shells, and the experimental data from Becker *et al* [32] and Lindle et al. [34] for the $4d$ shell. Good agreement between the two calculations can be seen for the $5p$ and $4d$ sub-shells. However, the Cooper minimum of the $5s$ shell is displaced between the two calculations.

On the middle panel of Fig. 4 we display the partial photoionization phase shifts in the $5s$, $5p$ and $4d$ sub-shells of Xe calculated in the same two models. Here agreement is not so straightforward as for the cross-section.

On the bottom panel of Fig. 4 the phase shifts are converted into photoemission time delays according to Eq. (6). The time delays are qualitatively similar in the two models. However, some important differences can be clearly seen. More specifically, the Cooper minimum shift of the $5s$ sub-shell is seen very clearly.

B. Inter-shell time delay difference

In this section, we present the results of our calculations of time delay difference between the $2s$ and $2p$ shells in Ne and $3s$ and $3p$ shells in Ar.

1. Neon

The time delay difference between the $2s$ and $2p$ sub-shells of Ne is shown in Fig. 5. This difference is fairly large near the $2s$ threshold, indicative of the fact that the low energy $2s$ photoelectron takes longer time to exit compared to the higher energy $2p$ electron. As the photon energy increases, it is the photoelectron time delay in the $2p$ shell which is smaller than that of the $2s$ sub-shell.

The *measured value* of the time delay between photoionization channels from the $2s$ and $2p$ sub-shells of neon at the photon energy of 100 eV is 21 ± 10 as [5]. The RRPA prediction is about 10 as which is only half of the experimental value. It is smaller in comparison to the large time delay difference in the near threshold region. It seems that the contribution to the experimentally measured time delay comes from two processes: (i) the delay *difference* in the single photon ionization channel and (ii) the time delay associated with two-photon ionization channel, sometimes referred to as the continuum-continuum (CC) [6] or Coulomb-laser coupling (CLC) [35] corrections. The RRPA accounts for the part of the time-delay, associated with the single photon process. However, the CC, or equivalently CLC, correction accounts for only 3.5 as [35] and cannot reconcile the difference between the measured and calculated time delay difference between the $2s$ and $2p$ shells. Similar conclusions were reached in previous numerical studies [15–18]

2. Argon

The time delay difference between the 3s and 3p sub-shells of Ar is given in Fig. 6. Near the $3s$ threshold, the $3s$ electrons escape somewhat more slowly compared to the $3p$ electrons. The rapid change in the scattering phase shift near the Cooper minimum affects the time delay between the $3s$ and $3p$ electrons.

The time delay predicted by the RRPA is compared with those measured by Klünder *et al* [4]. From the experimental results, time delay for the single photon ionization channel is extracted and plotted. There is fairly good agreement between the RRPA result and experimental observations. Near the Cooper minimum, the experimental result shows an enhancement in time delay, in response to the presence of Cooper minimum. Unfortunately, there is a scarcity of experimental data to verify the behaviour of time delay near the Cooper minimum region.

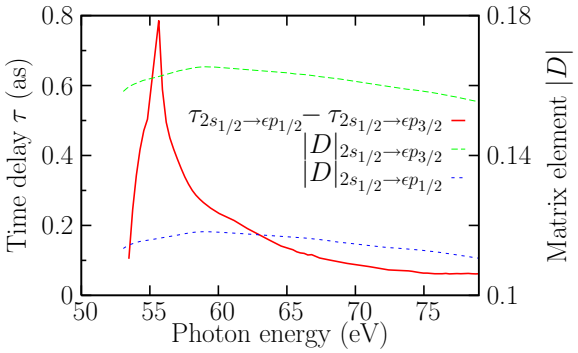

FIG. 7: (Color online) The time delay difference between the two relativistic channels $2s_{1/2} \to \epsilon p_{1/2}$ and $2s_{1/2} \to \epsilon p_{3/2}$ in neon (red solid line, left y-axis). The moduli of the corresponding transition matrix elements are plotted with the blue dotted and green dashed lines, respectively (right y-axis).

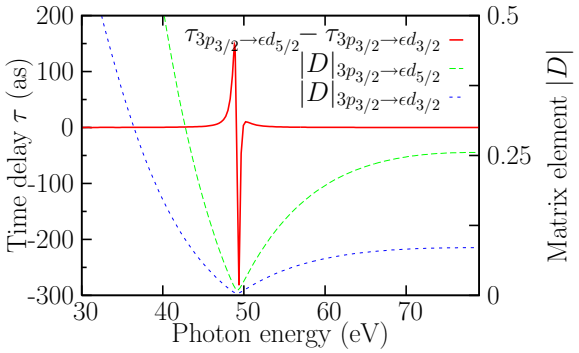

FIG. 8: (Color online) The time delay difference between the two relativistically split channels $3p_{3/2} \to \epsilon d_{3/2}$ and $3p_{3/2} \to \epsilon d_{5/2}$ in Ar (red solid line, left y-axis). The moduli of the corresponding transition matrix elements are plotted with the blue dotted and green dashed lines, respectively (right y-axis).

C. Inter-channel time delay difference

In this section, we show our results for the time delay difference between the two relativistically split channels. This difference is particularly strong near the Cooper minima in the respective photoionization cross-sections.

1. Neon

The neon $2s$ photoionization cross-section, shown in Fig. 7, does not have a Cooper minimum which is displaced to the discrete part of the spectrum. Hence, the cross-section increases gradually from the threshold. Nevertheless, the hidden Cooper minimum causes a noticeable time-delay difference between the two relativistic channels $2s_{1/2} \to \epsilon p_{1/2}$ and $2s_{1/2} \to \epsilon p_{3/2}$. Calculations were done at a number of energy points and the sharp structure therefore may not be just numerical noise. It might be due to a slight difference in the positions of the Cooper minima, even though they are in the discrete spectrum

2. Argon, krypton and xenon

In Fig. 8 we show the time delay difference between the two relativistically split channels $3p_{3/2} \to \epsilon d_{3/2}$ and $3p_{3/2} \to \epsilon d_{5/2}$. Near the $3p_{3/2} \to \epsilon d_{3/2}$ Cooper minimum, this time delay difference is positive, whereas it is negative near the $3p_{3/2} \to d_{5/2}$ Cooper minimum. The Cooper minima positions are indicated by the moduli plot of the corresponding transition matrix elements. The strong variation of the time delay difference indicates the importance of employing a relativistic formalism.

The time delay of photoemission relative to absorption of the photon in the $3p_{3/2} \to \epsilon d_{5/2}$ channel occurs somewhat (a few hundreds of attoseconds) later than in the $3p_{3/2} \to \epsilon d_{3/2}$ channel into the region of the $3p_{3/2} \to \epsilon d_{3/2}$ Cooper minimum. Here, $3p_{3/2} \to \epsilon d_{3/2}$ is the quicker exit channel. Likewise, photoionization in the $3p_{3/2} \to \epsilon d_{3/2}$ channel occurs somewhat later than in the $3p_{3/2} \to \epsilon d_{5/2}$ channel into the region of $3p_{3/2} \to \epsilon d_{5/2}$ Cooper minimum. Here, $3p_{3/2} \to \epsilon d_{3/2}$ is the slower exit channel.

Very similar tendencies in the inter-channel time delay difference near the respective Cooper minima can be seen in Fig. 9 for Kr and in Fig. 10 for Xe. Owing to increasing spin-orbit splitting, the difference in the Cooper minima positions is larger in these heavier atoms and, therefore, the inter-channel time delay difference is more prominent.

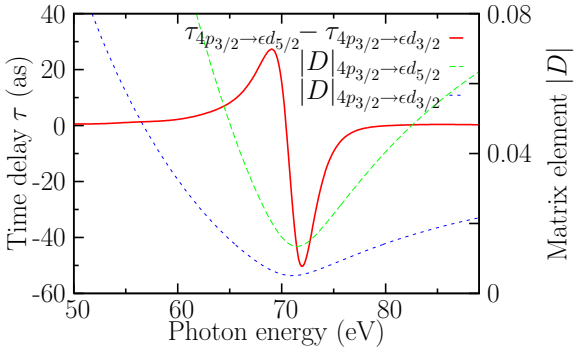

FIG. 9: Same as in Fig. 8 for the relativistically split channels $4p_{3/2} \to \epsilon d_{3/2}$ and $4p_{3/2} \to \epsilon d_{5/2}$ in Kr.

IV. CONCLUSIONS

In the present work, the photoelectron group time delay in valence shell photoionization of the noble gas atoms of Ne, Ar, Kr, and Xe were theoretically studied within the framework of the fully relativistic RRPA methodology. Moreover, for a better understanding of

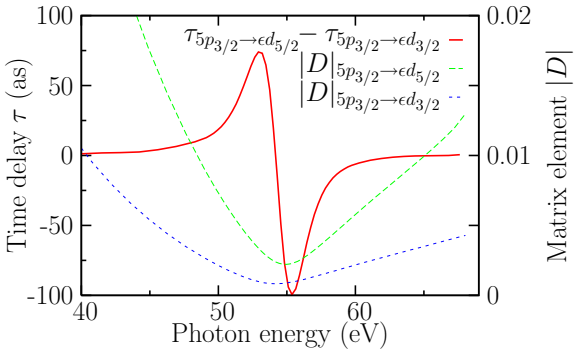

FIG. 10: Same as in Fig. 8 for the relativistically split channels $5p_{3/2} \to \epsilon d_{3/2}$ and $5p_{3/2} \to \epsilon d_{5/2}$ in Xe.

the importance of relativistic effects, a comparison was performed between corresponding non-relativistic RPAE calculations [17]. In addition, to control the accuracy of the present results, comparison was made with available experimental data for the partial photoionization cross sections and inter-shell time delays. It was demonstrated that relativistic effects manifest themselves particularly strongly near a Cooper minimum where a large difference in time delay was revealed between spin-orbit split exit channels. Specifically, it was found that, near a Cooper minimum in the $np_{3/2} \to \epsilon d_{3/2}$ channel, a photoelectron leaves the atom quicker *via* the $np_{3/2} \to \epsilon d_{3/2}$ channel than *via* the $np_{3/2} \to \epsilon d_{5/2}$ channel and vice verse. Furthermore, it was discovered that the time-delay difference between two relativistically split exit channels is largest for Ar (about two hundred as), smallest in Kr (about 30 as) and intermediate (about 50 as) for Xe. Further studies are necessary to determine if there is any systematic trend in the time-delay phenomenon along a sequence of atoms with progressively increasing atomic numbers. Inclusion of the non-dipole terms to the interaction Hamiltonian, as in Ref. [36], is also desirable for the completeness of the study.

V. ACKNOWLEDGMENTS

This work was supported by the Department of Science and Technology (DST), Government of India, by the National Science Foundation, by the Department of Energy, Office of Chemical Sciences, and by the Australian Research Council. One of the authors (Jobin Jose) is thankful to IIT-Mandi for the hospitality and support he received for a part of this work that was done at Mandi

[1] A. Baltuška *et al*, *Attosecond control of electronic processes by intense light fields*, Nature **421**, 611 (2003).
[2] R. Kienberger *et al*, *Atomic transient recorder*, Nature **427**, 817 (2004).
[3] P. Eckle *et al*, *Attosecond angular streaking*, Nat. Phys. **4**, 565 (2008).
[4] K. Klünder *et al*, *Probing single-photon ionization on the attosecond time scale*, Phys. Rev. Lett. **106**(14), 143002 (2011).
[5] M. Schultze *et al*, *Delay in Photoemission*, Science **328**(5986), 1658 (2010).
[6] D. Guénot, K. Klünder, C. L. Arnold, D. Kroon, J. M. Dahlström, M. Miranda, T. Fordell, M. Gisselbrecht, P. Johnsson, J. Mauritsson, et al., *Photoemission-time-delay measurements and calculations close to the 3s-ionization-cross-section minimum in ar*, Phys. Rev. A **85**, 053424 (2012).
[7] D. Guénot, D. Kroon, M. Kotur, E. Balogh, E. W. Larsen, J. M. Dahlstr.m, J. Mauritsson, M. Gisselbrecht, E. Lindroth, K. Varju, et al., *Measurements of photoemission time delays in noble gas atoms*, J. Phys. B p. submitted (2014).
[8] C. Palatchi, J. M. Dahlström, A. S. Kheifets, P. Agostini, and L. F. DiMauro, *Atomic delay in helium, neon, argon and krypton*, J. Phys. B p. submitted (2014).
[9] S. B. Schoun, R. Chirla, J. Wheeler, C. Roedig, P. Agostini, L. F. DiMauro, K. J. Schafer, and M. B. Gaarde, *Attosecond pulse shaping around a cooper minimum*, Phys. Rev. Lett. **112**, 153001 (2014).
[10] L. Eisenbud, Ph.D. thesis, Princeton University (1948).
[11] E. P. Wigner, *Lower limit for the energy derivative of the scattering phase shift*, Phys. Rev. **98**(1), 145 (1955).
[12] H. Friedrich, *Theoretical Atomic Physics* (Springer-Verlag, Berlin, 2006).
[13] F. T. Smith, *Lifetime matrix in collision theory*, Phys. Rev. **118**, 349 (1960).
[14] A. S. Kheifets and I. A. Ivanov, *Delay in atomic photoionization*, Phys. Rev. Lett. **105**(23), 233002 (2010).
[15] L. R. Moore, M. A. Lysaght, J. S. Parker, H. W. van der Hart, and K. T. Taylor, *Time delay between photoemission from the 2p and 2s subshells of neon*, Phys. Rev. A **84**, 061404 (2011).
[16] J. M. Dahlström, T. Carette, and E. Lindroth, *Diagrammatic approach to attosecond delays in photoionization*, Phys. Rev. A **86**, 061402 (2012).
[17] A. S. Kheifets, *Time delay in valence-shell photoionization of noble-gas atoms*, Phys. Rev. A **87**, 063404 (2013).
[18] J. Feist, O. Zatsarinny, S. Nagele, R. Pazourek, J. Burgdörfer, X. Guan, K. Bartschat, and B. I. Schneider, *Time delays for attosecond streaking in photoionization of neon*, Phys. Rev. A **89**, 033417 (2014).
[19] P. C. Deshmukh, D. Angom, and A. Banik, *Atomic and Molecular Physics DST-SERC school* (Narosa Publication House, New Delhi, 2012), chap. Symmetry in Electron-Atom Collision and Photoionization Process, lectures at Birla Institute of Technology.
[20] W. R. Johnson and C. D. Lin, *Multichannel relativistic random-phase approximation for the photoionization of atoms*, Phys. Rev. A **20**, 964 (1979).
[21] A. Derevianko, W. Johnson, and K. Cheng, *Non-dipole effects in photoelectron angular distributions for rare gas atoms*, Atomic data and nuclear data tables **73**(2), 153

(1999), ISSN 0092-640X.

[22] Y. Ralchenko, A. E. Kramida, J. Reader, and NIST ASD Team, *NIST Atomic Spectra Database (version 3.1.5)*, Tech. Rep., National Institute of Standards and Technology, Gaithersburg, MD. (2011), URL `http://physics.nist.gov/asd`.

[23] M. Y. Amusia and N. A. Cherepkov, *Many-Electron Correlations in the Scattering Processes* (North-Holland, Amsterdam, 1975), vol. 5 of *Case Studies in Atomic Physics*, pp. 47 –179.

[24] M. Y. Amusia and L. V. Chernysheva, *Computation of atomic processes : A handbook for the ATOM programs* (Institute of Physics Pub., Bristol, UK, 1997).

[25] J. Bizau and F. Wuilleumier, *Redetermination of absolute partial photoionization cross sections of he and ne atoms between 20 and 300 eV photon energy*, Journal of Electron Spectroscopy and Related Phenomena **71**(3), 205 (1995), ISSN 0368-2048.

[26] B. Möbus *et al*, *Measurements of absolute Ar 3s photoionization cross sections*, Phys. Rev. A **47**(5), 3888 (1993).

[27] J. Samson and W. Stolte, *Precision measurements of the total photoionization cross-sections of He, Ne, Ar, Kr, and Xe*, J. Electr. Spectr. Relat. Phenom. **123**(2-3), 265 (2002).

[28] U. Fano and J. W. Cooper, *Spectral distribution of atomic oscillator strengths*, Rev. Mod. Phys. **40**, 441 (1968).

[29] M. Y. Amusia, V. K. Ivanov, N. A. Cherepkov, and L. V. Chernysheva, *Interference effects in photoionization of noble gas atoms outer s-subshells*, Physics Letters A **40**(5), 361 (1972).

[30] A. Ehresmann, F. Vollweiler, H. Schmoranzer, V. L. Sukhorukov, B. M. Lagutin, I. D. Petrov, G. Mentzel, and K. H. Schartner, *Photoionization of Kr* 4*s. III. Detailed and extended measurements of the Kr* 4*s-electron ionization cross section*, J. Phys. B **27**(8), 1489 (1994).

[31] S. Aksela, H. Aksela, M. Levasalmi, K. H. Tan, and G. M. Bancroft, *Partial photoionization cross sections of Kr* 3*d,* 4*s, and* 4*p levels in the photon energy range 37-160eV*, Phys. Rev. A **36**, 3449 (1987).

[32] U. Becker *et al*, *Subshell photoionization of Xe between 40 and 1000 eV*, Phys. Rev. A **39**, 3902 (1989).

[33] A. Fahlman, M. O. Krause, T. A. Carlson, and A. Svensson, *Xe* 5*s,* 5*p correlation satellites in the region of strong interchannel interactions, 28-75 eV*, Phys. Rev. A **30**, 812 (1984).

[34] D. W. Lindle, T. A. Ferrett, P. A. Heimann, and D. A. Shirley, *Photoemission from xe in the vicinity of the 4d cooper minimum*, Phys. Rev. A **37**, 3808 (1988).

[35] S. Nagele, R. Pazourek, J. Feist, K. Doblhoff-Dier, C. Lemell, K. Tökési, and J. Burgdörfer, *Time-resolved photoemission by attosecond streaking: extraction of time information*, J. Phys. B **44**(8), 081001 (2011).

[36] I. A. Ivanov and A. S. Kheifets, *Relativistic effects in time delay of atomic photoionization*, Phys. Rev. A **89**, 043405 (2014).